Reprinted from **Applied Optics**, Vol. 22, page 2951, October 1, 1983

Retrieval of the optical properties of aerosols from aureole and extinction data

Teruyuki Nakajima, Masayuki Tanaka, and Toyotato Yamauchi

Solution of the small-angle approximation of Weinman *et al.*[1] is piled on the solution of the truncation approximation to synthesize the intensity field in the solar aureole. Accuracy within ±3% is attained for almost all parts of the sky and for air masses less than ~5. An iterative algorithm utilizing this calculation scheme is applied to the spectral aureole and extinction measurements to estimate the forward parts of the aerosol phase functions and to retrieve the aerosol volume spectra from them.

I. Introduction

Simplified calculation schemes of radiative transfer have been developed by Weinman *et al.*[1] and by Box and Deepak[2] to estimate the intensity distribution in the aureole region. By these methods, the almucantar intensity of the solar aureole can be obtained with sufficient accuracy when the solar elevation is high and the dust loading is moderate. However, the calculation error of the small-angle approximation method of Weinman *et al.* increases when multiple scattering by molecules prevails. On the other hand, calculation error of the MS approximation of Box and Deepak increases when the aerosol loading increases. In both methods, the accuracy of calculation decreases with increasing air mass.

To compensate these shortcomings, we have extended the theory of Box and Deepak to allow the solution of the small-angle approximation, by adding the solution of the small-angle approximation to the solution of the radiative transfer equation with a truncated phase function.[3,4]

It has been expected that the aerosol volume spectrum can be retrieved more accurately from simultaneous measurements of the aureole intensity and the atmospheric extinction than either single measurement.[5,6] Section IV of this paper is devoted to development of such a simultaneous inversion method. The forward part of the aerosol phase function is retrieved from measured aureole intensity by an iterative regression by use of our calculation scheme mentioned above. Although the absolute accuracy of the retrieved phase function depends considerably on the atmospheric turbidity, the relative shape of the phase function can be retrieved for any atmospheric turbidity condition. Since the calibration error of an aureole meter affects the accuracy of the inversion process,[7] we adopt an inversion method in which only relative values of the phase function are required. The absolute scale is given from simultaneous extinction measurements.

II. Truncation Approximation of the Radiative Transfer Equation

The main difficulty in the calculation of the aureole intensity is an increase of computational time and of instability due to a strong anisotropy of the aerosol phase function. For example, the dimension of the reflection and transmission matrices must be as large as ~(30 × 30) in the matrix method to calculate the spike of the intensity distribution in the solar aureole.[8] To simplify the computation it is conventional to decompose the phase function into the forward spike and the residue

$$P = f\hat{P} + (1 - f)P^*, \tag{1}$$

where f is the so-called truncation ratio. Correspondingly, we can decompose the field intensity into the spike in the solar aureole and its residue

$$I = \hat{I} + I^*, \tag{2}$$

which satisfy the transfer equations

T. Nakajima and M. Tanaka are with Tohoku University, Upper Atmosphere Research Laboratory, Sendai 980, Japan; T. Yamauchi is with Japan Meteorological Agency, Tokyo 100, Japan.
Received 9 April 1983.
0003-6935/83/192951-09$01.00/0.

$$\mu \frac{d\hat{I}}{d\tau} = -\hat{I} + \omega_0 f \int_0^{2\pi} d\phi' \int_{-1}^{1} d\mu' \hat{P}(\tau,\mu,\mu',\phi - \phi')\hat{I}(\tau,\mu',\phi'), \tag{3}$$

$$\mu \frac{dI^*}{d\tau} = -I^* + \omega_0(1-f) \int_0^{2\pi} d\phi' \int_{-1}^{1} d\mu' P^*(\tau,\mu,\mu',\phi - \phi')I^*(\tau,\mu',\phi')$$
$$+ \omega_0 \int_0^{2\pi} d\phi' \int_{-1}^{1} d\mu' [f\hat{P}(\tau,\mu,\mu',\phi - \phi')I^*(\tau,\mu',\phi')$$
$$+ (1-f)P^*(\tau,\mu,\mu',\phi - \phi')\hat{I}(\tau,\mu',\phi')], \tag{4}$$

where μ and ϕ are, respectively, the cosine of the nadir angle and the azimuthal angle of the direction of radiation, and ω_0 and τ are the single scattering albedo and the optical thickness of the atmosphere, respectively. It is worthwhile to note that, if the third and fourth terms on the right-hand side of Eq. (4) are transferred to the right hand-side of Eq. (3), the resultant equations are the same as those of Deirmendjian[9] and of Box and Deepak.[2] The idea of the truncation method[3,4,10,11] is to approximate $\hat{P}$ and $\hat{I}$ by the Dirac delta function. In this approximation, the solution of Eq. (3) can be obtained analytically, and Eq. (4) is reduced to the ordinary transfer equation with transformed variables

$$d\tau^* = (1 - f\omega_0)d\tau, \qquad \omega_0^* = \frac{1-f}{1-f\omega_0}\omega_0. \tag{5}$$

Since the anisotropy of the involved phase function is reduced to a considerable degree, the solution of Eq. (4) can be obtained more easily than the original transfer equation. Potter[4] pointed out in his numerical experiment that "in general the approximation gave results that were accurate to within 1% for widely differing values of the incident angle, optical depth and absorption. Larger errors appear when the incident or emergent angle is within ~5° of the grazing angle $\theta_0 = 90°$ and, in the case of the transmitted intensity, when the incident and emission angles are nearly equal." In this truncation approximation the spike of the intensity distribution in the solar aureole is given as a delta function. Our expectation is that a better approximation will be attained if we utilize a more realistic solution of Eq. (3) instead of the delta function.

Since the truncation ratio f is in general much smaller than unity, the effective single scattering albedo in Eq. (3), $\omega_0 f$, is also of small value and, accordingly, single scattering contributes predominantly to the solution of Eq. (3). Then the single scattering approximation is expected to give a good solution of Eq. (3). The MS approximation of Box and Deepak[2] is obtained if we interpret $\hat{P}$ and P^* in Eq. (1) as phase functions for aerosols and molecules, respectively, and neglect the third and fourth terms on the right-hand side of Eq. (4). In this paper we start with an alternative solution of Eq. (3) given by Weinman *et al.*[1] Following Weinman *et al.* we translate the polar coordinate of the direction of radiation as shown in Fig. 1, or

$$\mu \simeq \mu_0 + \sqrt{1-\mu_0^2}\,\Psi\cos\Phi, \qquad \phi \simeq \Psi\sin\Phi/\sqrt{1-\mu_0^2}, \tag{6}$$

retaining the first-order terms of Ψ. If we further decompose $\hat{I}$ into direct and diffuse intensities and rewrite the latter as $\hat{I}$, the transfer equation for $\hat{I}$ is given by

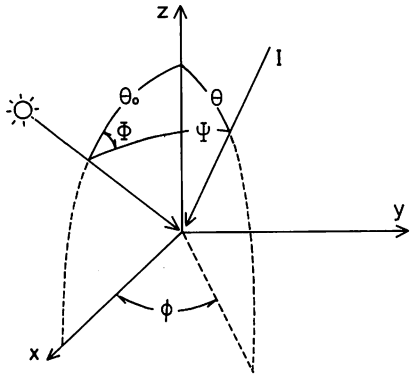

Fig. 1. Definition of angles.

$$\left(1 + \frac{\sqrt{1-\mu_0^2}}{\mu_0}\Psi\cos\Phi\right)\frac{d\hat{I}}{d\hat{\tau}} = -\hat{I}$$
$$+ \hat{\omega}_0 \int_0^{2\pi} d\Phi' \int_0^{\epsilon} \Psi' d\Psi' \hat{P}$$
$$\times (\sqrt{\Psi^2 - 2\Psi\Psi'\cos(\Phi - \Phi') + \Psi'^2})\hat{I}(\hat{\tau},\Psi',\Phi')$$
$$+ \hat{\omega}_0\hat{P}(\Psi)\exp(-\hat{\tau}), \tag{7}$$

where

$$d\hat{\tau} = d\tau/\mu_0, \qquad \hat{\omega}_0 = \omega_0 f, \tag{8}$$

and ϵ is a small value. Using the symmetry properties of $\hat{I}$ and $\hat{P}$ with respect to Φ, we can expand $\hat{I}$ and $\hat{P}$ into the following cosine series:

$$\hat{I}(\hat{\tau},\Psi,\Phi) = \sum_{m=0}^{\infty} \hat{I}^{(m)}(\hat{\tau},\Psi)\cos m\Phi,$$
$$\hat{P}(\Psi,\Psi',\Phi) = \sum_{m=0}^{\infty} \hat{P}^{(m)}(\Psi,\Psi')\cos m\Phi. \tag{9}$$

Taking the first two terms of expansion of Ψ, the following two equations are obtained for scattering in the aureole region:

$$\frac{d\hat{I}^{(0)}}{d\hat{\tau}} = -\hat{I}^{(0)} + \hat{\omega}_0\hat{P}^{(0)}(\Psi)\exp(-\hat{\tau})$$
$$+ 2\pi\hat{\omega}_0 \int_0^{\infty} \Psi' d\Psi' \hat{P}^{(0)}(\Psi,\Psi')\hat{I}^{(0)}(\hat{\tau},\Psi'), \tag{10}$$

$$\frac{d\hat{I}^{(1)}}{d\hat{\tau}} = -\hat{I}^{(1)} - \frac{\sqrt{1-\mu_0^2}}{\mu_0}\Psi\frac{d\hat{I}^{(0)}}{d\hat{\tau}}. \tag{11}$$

The solution of Eq. (10) has been given by Weinman *et al.*[1] by expanding into the successive order of scattering and applying the Hankel transformation technique. In their method the phase function must be expanded by a sum of Gaussian functions. Then, the following Gaussian-Legendre expansion of the phase function is suitable for our approximation:

$$P = f \sum_{n=1}^{N} C_n \exp(-\Theta^2/E_n) + (1-f) \sum_{n=0}^{2M-1} \frac{2n+1}{4\pi} \chi_n^* P_n, \quad (12)$$

where P_n is the nth-order Legendre polynomial and χ_n^* is the Legendre expansion coefficient of P^*, which can be related to χ_n, the Legendre expansion coefficient of P by the delta-M method.[11] Constants E_n and C_n are determined to fit the residue $P - P^*$, i.e., $\hat{P}$ in Eq. (1), by a least-squares error technique. For $N = 5$ in Eq. (12), the solutions of Eqs. (10) and (11) are

$$\hat{I}^{(0)} + \hat{I}^{(1)} \cos\Phi = \sum_{n=1}^{\infty} \left[1 + \frac{\sqrt{1-\mu_0^2}}{\mu_0} \Psi \left(\frac{\hat{\tau}}{n+1} - 1\right) \cos\Phi\right] \times \frac{(\pi\hat{\omega}_0\hat{\tau})^n}{\pi} \exp(-\hat{\tau}) \sum_{m=0}^{n} \sum_{l=0}^{m} \sum_{k=0}^{l} \sum_{j=0}^{k} C_{nmlkj} \exp(-\Psi^2/\chi_{nmlkj})/\chi_{nmlkj}, \quad (13)$$

$$C_{nmlkj} = \frac{(E_1C_1)^{n-m}(E_2C_2)^{m-l}(E_3C_3)^{l-k}(E_4C_4)^{k-j}(E_5C_5)^j}{(n-m)!(m-l)!(l-k)!(k-j)!j!},$$

$$\chi_{nmlkj} = (n-m)E_1 + (m-l)E_2 + (l-k)E_3 + (k-j)E_4 + jE_5. \quad (14)$$

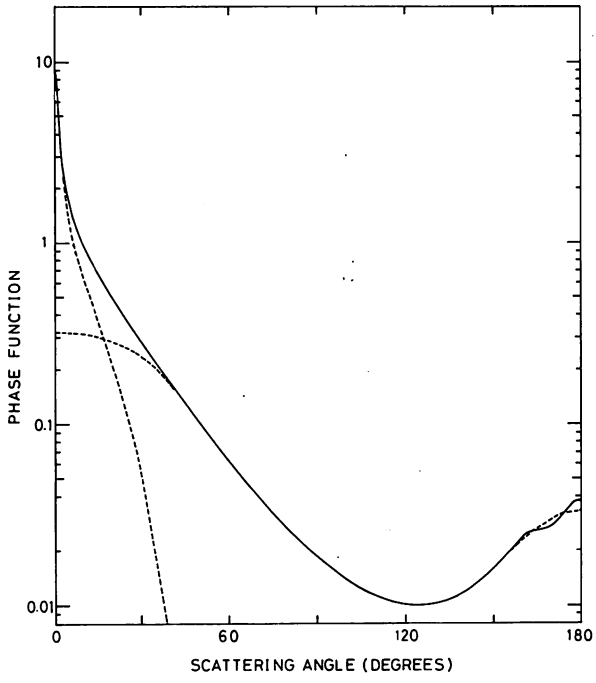

Fig. 2. Gaussian-Legendre fitting of the phase function of aerosols with Junge size distribution and $m = 1.50 - 0i$ at $\lambda = 0.35$ μm.

The numerical solution of Eq. (4) is obtained by a matrix operator method code developed by us for the atmosphere–ocean–land system.[6,12] For the number of discrete ray paths in the atmospheric hemisphere, we choose a value somewhat larger than M, say, $M + 3$.

Figure 2 and Table I show an example of the Gaussian-Legendre expansion of the phase function of aerosols with Junge size distribution and refractive index $m = 1.5 - 0i$ at wavelength $\lambda = 0.35$ μm. In this example, the values of N and M in Eq. (12) are adopted to be $N = M = 5$.

Table I. Values of the coefficients in Eq. (12) for the example shown in Fig. 2.

n	Cn	En	n	Xn
1	2.0824	4.0516E-5	0	1.000000
2	19.8831	2.8677E-4	1	0.580899
3	8.5543	2.0297E-3	2	0.348030
4	3.5127	1.4365E-2	3	0.133072
5	2.4513	1.0168E-1	4	0.055579
			5	0.001486
			6	-0.006693
			7	-0.010957
			8	-0.006083
			9	-0.002575
			f	0.278261

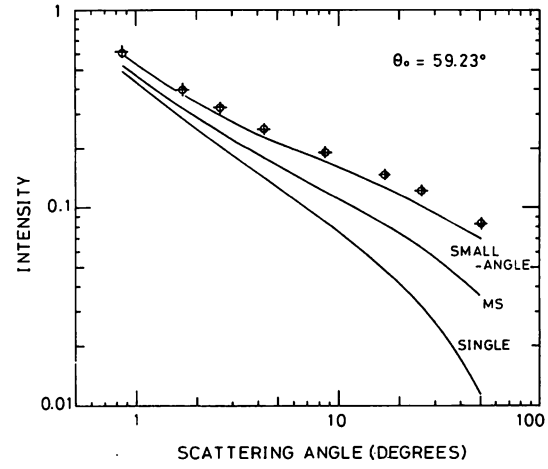

Fig. 3. Almucantar intensity of a turbid atmosphere for $\lambda = 0.35$ μm, $\theta_0 = 59.23°$, $\tau_a = 1.066$, $\tau_m = 0.636$, and the aerosol phase function shown in Fig. 2. The true values and the truncation approximation are shown by circles and crosses, respectively. The single scattering, the small-angle, and the MS approximations are shown by lines labeled *SINGLE*, *SMALL-ANGLE*, and *MS*, respectively.

Figure 3 shows the almucantar intensity in the solar aureole as a function of the scattering angle Θ for the aerosol phase function shown in Fig. 2 and $\lambda = 0.35$ μm, $\theta_0 = 59.23°$, $\tau_a = 1.066$, and $\tau_m = 0.636$, where τ_a and τ_m are optical thicknesses of aerosols and molecules, respectively. The true values are calculated by the matrix operator method code developed by Arao[8] for the aureole calculation, whereas the truncation solution of Eq. (4) is solved by taking the value of M in Eq. (12) to be 5. The effect of multiple scattering is significant in this example and the small-angle and the MS approximations underestimate the intensity, whereas the truncation approximation follows accurately the true values. Maximum and root mean square errors of the truncation approximation are 2.5 and 1.6%, respectively, which are mainly due to the fitting error involved in the finite sum approximation of the aerosol phase function by Gaussian functions. The use of more sophisticated techniques of exponential sum fitting[13] will improve the accuracy of the truncation approximation. In this context the solution of Eq. (3) by expanding into successive orders of scattering has an advantage for the small-angle approximation since it needs no fitting such as Eq. (12).

Table II. Almucantar intensities for the turbid atmosphere with aerosols obeying the Junge size distribution and for $\theta_0 = 59.23°$.

		$\lambda = 0.35$	$\tau_a = 0.133$ $\tau_m = 0.636$		$\lambda = 0.50$	$\tau_a = 0.200$ $\tau_m = 0.145$	
Φ	Θ	TRUE	TRUNC	%-ERR	TRUE	TRUNC	%-ERR
0	0.00	0.6838	0.6840	0.0	1.471	1.473	0.1
1	0.86	0.4553	0.4622	1.5	1.155	1.154	-0.1
2	1.72	0.2955	0.2938	-0.6	0.7439	0.7451	0.2
3	2.58	0.2353	0.2362	0.4	0.5554	0.5532	-0.4
5	4.30	0.1838	0.1845	0.4	0.3919	0.3884	-0.9
10	8.59	0.1397	0.1404	0.5	0.2516	0.2522	0.2
20	17.16	0.1097	0.1110	1.1	0.1576	0.1582	0.4
30	25.70	0.0944	0.0952	0.9	0.1122	0.1121	-0.1
60	50.89	0.0699	0.0706	0.9	0.0521	0.0519	-0.5

Table III. Circumsolar intensity in the vertical plane involving the sun for $\lambda = 0.35$ μm and $\theta_0 = 3.18°$.

		$\lambda = 0.35$	$\tau_a = 0.133$ $\tau_m = 0.636$	
θ	Θ	TRUE	TRUNC	%-ERR
7.25	4.07	0.1866	0.1851	-0.8
11.24	8.06	0.1391	0.1374	-1.2
15.07	11.89	0.1210	0.1205	-0.4
18.68	15.50	0.1108	0.1105	-0.3
22.01	18.83	0.1042	0.1040	0.0

Two other examples of similar numerical tests are shown in Tables II and III, also for the cases of strong multiple scattering by aerosols or molecules. The aerosol model is the same as that in Fig. 3. The maximum and root mean square errors of the results shown are 1.5 and 0.7%, respectively. The accuracy of the truncation approximation is better for clearer atmospheres than that for the examples shown, since the sum of the solution of Eqs. (3) and (4), i.e., $\hat{I} + I^*$, approaches the solution of the single scattering approximation of the original transfer equation by decreasing the optical thickness of the atmosphere.

Figure 4 shows the almucantar intensity as a function of the azimuthal angle for $\lambda = 0.5$ μm, $\tau_m = 0.15$ and various values of air mass ξ ($= 1/\mu_0$) and of M in Eq. (12). The upper and lower lines are for $\tau_a = 0.50$ and 1.0, respectively. The aerosol model is the same as for other examples. The values calculated with $M = 17$ closely coincide with the true values. From the figure we can see that the truncation approximation gives sufficiently accurate values for various turbidity conditions and air masses if we adopt the M value a little larger than 5. The maximum and root mean square errors are 2.42 and 0.87% for $\tau_a = 0.50$ and 3.01 and 1.45% for $\tau_a = 1.0$. In more detail, the truncation approximation overestimates more or less the intensity, increasingly with increasing optical thickness.[14] The error also increases in the region of scattering angles where the contributions of $\hat{P}$ and P^* are of the same order of magnitude. It is also noted that the perturbation solution, Eq. (13), gives realistic solution only near the almucantar for large air masses, since it involves the term $1/\mu_0$.

Hereafter we adopt $M = 7$ and calculate the almucantar intensity in the aureole region.

III. Retrieval of the Phase Function

In this and following sections we discuss the inversion of the aerosol volume spectrum from the aureole and the extinction data. For such an inversion, we first have to obtain the single scattering phase function from actual aureole data. We adopt an iterative regression algorithm to subtract the multiply scattered intensity. Simultaneous measurements of the optical thickness (i.e., extinction measurements) are necessary for this algorithm.

The initial value of the aerosol phase function is given as follows:

$$P_a^1(\Theta) = \begin{cases} I^0(\mu,\phi), & \text{for } \Theta \le \Theta_{max}, \\ P_a^0(\Theta), & \text{for } \Theta > \Theta_{max}, \end{cases} \tag{15}$$

where I^0 is the measured aureole intensity for scattering angles $\Theta \le \Theta_{max}$, and P_a^0 is a function by which the phase function is extrapolated for scattering angles $\Theta > \Theta_{max}$. Thus, the total phase function is constructed by

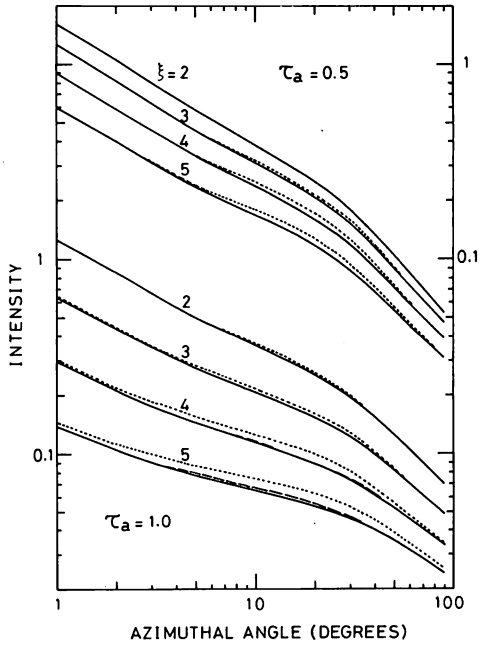

Fig. 4. Almucantar intensities for various values of ξ and M. Dotted, broken, and solid lines are, respectively, for $M = 5$, 7, and 17. The left- and right-side scales are for the upper and lower lines, respectively.

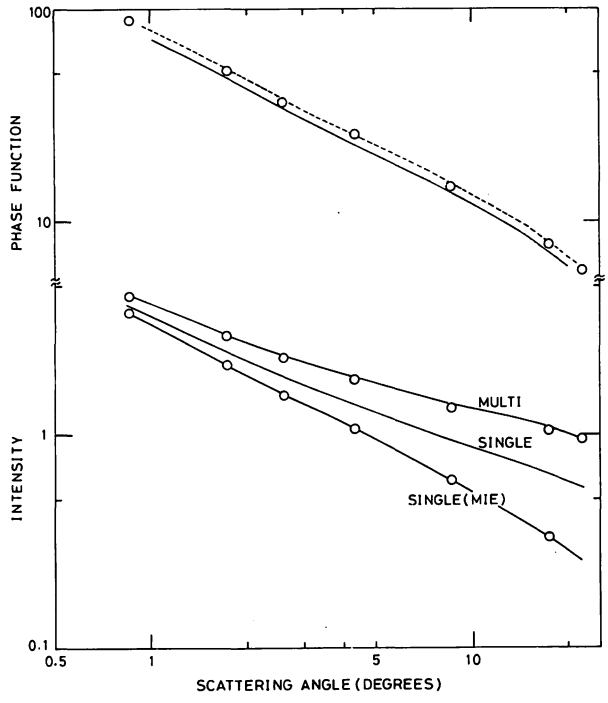

Fig. 5. Almucantar intensity (lower part) and the phase function (upper part) for $\lambda = 0.35\ \mu m$, $\theta_0 = 59.23°$, $\tau_a = 0.133$ and $\tau_m = 0.636$. Lines and circles correspond to the true and the retrieved values, respectively. Lines labeled *MULTI*, *SINGLE*, and *MIE* are the total intensity, singly scattered intensity, and intensity singly scattered by aerosols, respectively.

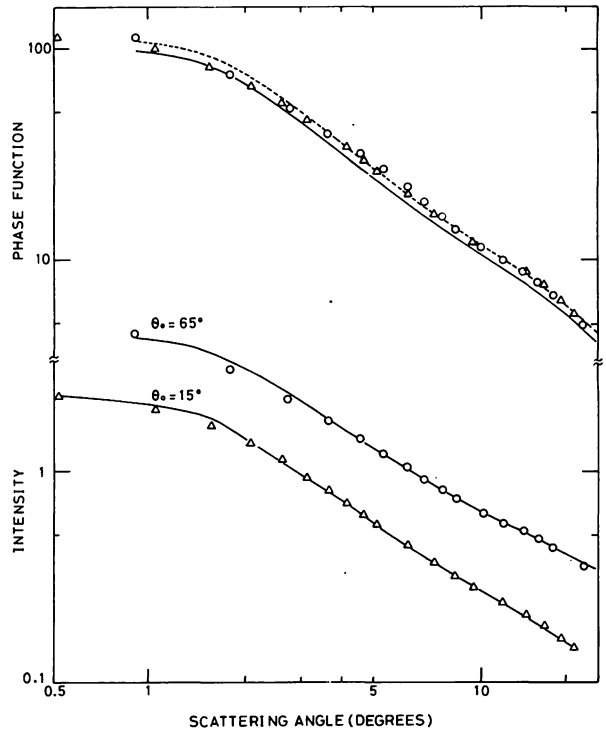

Fig. 6. Same as in Fig. 5 but for a different aerosol model (see the text). Two values are assumed for the solar zenith angle, i.e., 15° and 65°, and for clear display the intensity scale for $\theta_0 = 65°$ is shifted by a factor of 2.

$$P^n(\Theta) = \frac{\omega_{0a}\tau_a}{\omega_{0a}\tau_a + \tau_m} P_a^n(\Theta) \Big/ \left[2\pi \int_{-1}^{1} d\cos\Theta P_a^n(\Theta)\right] + \frac{\tau_m}{\omega_{0a}\tau_a + \tau_m} \frac{3}{16\pi}(1 + \cos^2\Theta), \quad (16)$$

where ω_{0a} is the single scattering albedo of aerosols. Using the above optical variables, we can calculate the aureole intensity, I^n, by the truncation approximation given in the preceding section. An improved phase function of aerosols is then given by

$$P_a^{n+1}(\Theta) = r^n(\Theta) P_a^n(\Theta), \quad (17)$$

where the ratio $r^n(\Theta)$ is defined by

$$r^n(\Theta) = \begin{cases} I^0(\mu,\phi) I^n(\mu_{max},\phi_{max}) / [I^0(\mu_{max},\phi_{max}) I^n(\mu,\phi)], & \text{for } \Theta \le \Theta_{max}, \\ 1, & \text{for } \Theta > \Theta_{max}. \end{cases} \quad (18)$$

Repeating Eqs. (16) and (17), we can successively obtain a new phase function with which the observed intensity distribution is reconstructed more closely than in the previous step. It is found that six iterations are sufficient for most applications except for extremely noisy data; the maximum error of the ratio $r^n(\Theta)$ can usually be restricted to the limits of 5%. In the above iteration, unobservable variables such as $P_a^0(\Theta)$ and ω_{0a} are calculated by assuming a typical volume spectrum and the refractive index of aerosols.

Figure 5 shows an example of the numerical simulation. The aerosol model is the same as in Table II. The Junge size distribution and $m = 1.50 - 0.01i$ are adopted for the calculation of P_a^0 and ω_{0a}. The original phase function shifted parallel to the retrieved one is shown by a dashed line. As seen in the figure the relative profile of the phase function is retrieved fairly accurately, whereas the uncertainty involved in the absolute value of the retrieved phase function is as large as 10%. This is due to the fact that a more absorbing model is assumed for $P_a^0(\Theta)$ and ω_{0a} than that used in the original data; single scattering albedos of aerosols are 1.0 and 0.91 for the original data and for the model, respectively. A test run adopting an aerosol model with $m = 1.50 - 0i$ indicated that the retrieved phase function coincides closely with the true one. Figure 6 shows the result of another numerical simulation. Data are calculated for an aerosol model adopted by Weinman *et al.*[1] within the size range of $0.02 \le a \le 5.02\ \mu m$, $m = 1.54 - 0i$, $\tau_a = 0.50$, $\tau_m = 0.15$, and $\lambda = 0.50\ \mu m$. The same values are assumed for $P_a^0(\Theta)$ and ω_{0a} as in Fig. 5. Except for absolute values, the retrieved phase function follows closely the true value; errors are <4.1 and 5.4% for $\theta_0 = 15$ and 65°, respectively.

As seen from these examples the relative value of the aerosol phase function can be retrieved fairly well even if the optical properties of aerosols are guessed rather poorly. On the other hand, the absolute value of the phase function is less reliable, depending strongly on the assumed optical properties of aerosols. Since the absolute calibration of the aureole meter is also a matter of no small consideration, we shall consider an inversion

technique to retrieve the aerosol volume spectrum utilizing the multispectral phase functions obtained by the above mentioned scheme and normalized at an arbitrary scattering angle.

IV. Retrieval of the Aerosol Volume Spectrum

The inversion of the volume spectrum of aerosols from combined data of the aureole and the extinction measurements has been discussed theoretically by Shaw.[5] But the application of the theory to the observed data is still open to discussion. We have analyzed the observed spectral aureole data normalized at $\Theta = 5°$ or $10°$. By such a normalization, uncertainties in absolute calibration of the instrument as well as in the retrieval of the phase function discussed in the preceding section are mostly removed. We define the data vector as follows:

$$\mathbf{b} = \begin{bmatrix} C_1P(\Theta_1,\lambda_1) \\ C_1P(\Theta_2,\lambda_1) \\ \vdots \\ C_2P(\Theta_1,\lambda_2) \\ C_2P(\Theta_2,\lambda_2) \\ \vdots \\ \tau(\lambda_2) \\ \tau(\lambda_2) \\ \vdots \end{bmatrix}, \quad \mathbf{b}_0 = \begin{bmatrix} C_1P(\Theta_0,\lambda_1) \\ C_1P(\Theta_0,\lambda_1) \\ \vdots \\ C_2P(\Theta_0,\lambda_2) \\ C_2P(\Theta_0,\lambda_2) \\ \vdots \\ \tau(\lambda_0) \\ \tau(\lambda_0) \\ \vdots \end{bmatrix}, \tag{19}$$

where $P(\Theta,\lambda)$ and $\tau(\lambda)$ are, respectively, the phase function and the optical thickness observed at the scattering angle Θ and the wavelength λ; Θ_0 and λ_0 being the scattering angle and the wavelength at which the data are normalized, and the C_n are the calibration constants. Since these quantities relate linearly with the volume spectrum, $v(\ln a) = dV/d\ln a$, where a and V are particle radius and cumulative volume of particles, respectively, our problem is to solve the following linear equations:

$$\mathbf{b} + \boldsymbol{\epsilon} = \mathbf{L}\mathbf{V}, \qquad \mathbf{b}_0 + \boldsymbol{\epsilon}_0 = \mathbf{L}_0\mathbf{V}, \tag{20}$$

where $\boldsymbol{\epsilon}$ and $\mathbf{V}$ are the error vector and the vector of the volume spectrum, respectively, and $\mathbf{L}$ is the kernel matrix calculated from the Mie theory assuming spherical particles.[15] After normalizing the data vector, we define $\tilde{\mathbf{b}}$ and $\tilde{\boldsymbol{\epsilon}}$ as

$$\tilde{\mathbf{b}} + \tilde{\boldsymbol{\epsilon}} \equiv \frac{\mathbf{b} + \boldsymbol{\epsilon}}{\mathbf{b}_0 + \boldsymbol{\epsilon}_0} = \frac{\mathbf{L}\mathbf{V}}{\mathbf{L}_0\mathbf{V}}, \tag{21}$$

where the symbol / (or $*$) shows the dyadic operator of division (or multiplication) for vector elements. Introducing a crude estimation of the volume spectrum, $\mathbf{V}_c$, we transform Eq. (21) as follows:

$$\begin{aligned} \hat{\boldsymbol{\epsilon}} &\equiv \frac{\mathbf{L}_0\mathbf{V}}{\mathbf{L}_0\mathbf{V}_c} * \frac{\tilde{\boldsymbol{\epsilon}}}{\tilde{\mathbf{b}}} = \frac{\mathbf{L}_0\mathbf{V}}{\mathbf{L}_0\mathbf{V}_c} * \left(\frac{\mathbf{l}}{\tilde{\mathbf{b}}} * \frac{\mathbf{L}\mathbf{V}}{\mathbf{L}_0\mathbf{V}} - \mathbf{l}\right) \\ &= \frac{\mathbf{l}}{\mathbf{L}_0\mathbf{V}_c} * \left(\frac{\mathbf{l}}{\tilde{\mathbf{b}}} * \mathbf{L} - \mathbf{L}_0\right) * \mathbf{V}_c \frac{\mathbf{V}}{\mathbf{V}_c} \equiv \hat{\mathbf{L}}\hat{\mathbf{V}}, \end{aligned} \tag{22}$$

where $(\mathbf{l})_i = 1$ and

$$\hat{\mathbf{V}} = \frac{\mathbf{V}}{\mathbf{V}_c}, \tag{23}$$

$$\hat{\mathbf{L}} = \frac{\mathbf{l}}{\mathbf{L}_0\mathbf{V}_c} * \left(\frac{\mathbf{l}}{\tilde{\mathbf{b}}} * \mathbf{L} - \mathbf{L}_0\right) * \mathbf{V}_c. \tag{24}$$

The least-squares solution of Eq. (22) which allows a smoothing constraint to minimize the following square error:

$$E^2 = \hat{\boldsymbol{\epsilon}} \cdot \hat{\boldsymbol{\epsilon}} + \gamma(\hat{\mathbf{V}} - \mathbf{l}) \cdot (\hat{\mathbf{V}} - \mathbf{l}), \tag{25}$$

is given by[16]

$$\hat{\mathbf{V}} = (\hat{\mathbf{L}}^*\hat{\mathbf{L}} + \gamma\mathbf{I})^{-1}\gamma\mathbf{l}, \tag{26}$$

where $\mathbf{L}^*$ is the transpose of $\mathbf{L}$ and $\mathbf{I}$ is the unit matrix. It should be noted that the introduction of a homogeneous constraint in place of the second term of Eq. (25) leads the null solution because Eq. (22) is a homogeneous equation of the volume spectrum. The crude estimation of the volume spectrum in Eq. (23) is obtained from a two-parameter fitting of the aerosol optical thickness and of the aerosol phase function:

$$\tau_a = \beta\lambda^{3-p}, \qquad d\ln P/d\ln\Theta = -3.97\exp(-0.0509p^{2.5}), \tag{27}$$

which are obtained by the model calculation with Mie particles and the power-law volume spectrum of the form $v(\ln a) = C \times a^{4-p}$. In general, the most plausible value of the exponent $4 - p$ is different for the first and second equations. We therefore use the weighted mean of these two values.

The value of the refractive index of aerosols is also unknown in the above inversion problem. The possibility of simultaneous estimation of the volume spectrum and the complex refractive index of aerosols has been discussed by Tanaka *et al.*[15] but from the polar nephelometer data. Figure 7 shows the results of a similar analysis for the data of aureole–extinction combined measurements. In the figure, the root mean square deviation of the reconstructed data from the

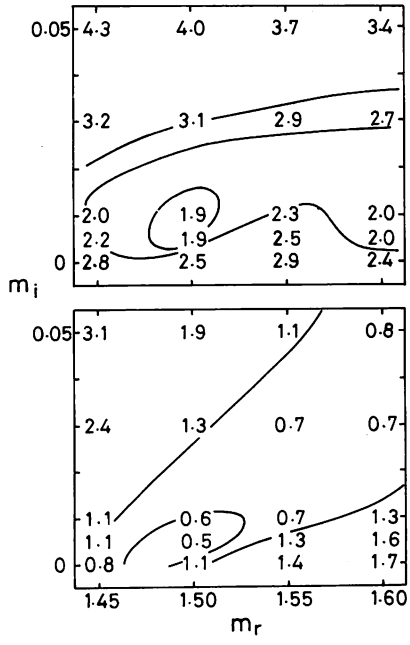

Fig. 7. Reconstruction errors in percent of the optical data as functions of the real and imaginary parts of the refractive index. The upper and lower figures are for a bimodal and the Junge volume spectra, respectively.

observed data is shown as a function of the real and imaginary parts of the refractive index, m_r and m_i. The simulated data are calculated for a bimodal and the Junge-type volume spectra with $m = 1.50 - 0.01i$. The values of the scattering angle are assumed to be 0.0, 0.6, 0.8, 1.0, 1.25, 1.50, (0.5), 4.0, (1), 8, 10, 12, 15, 20, and 25 for the aureole data. The wavelengths are adopted as 0.369, 0.560, 0.788, and 1.040 μm for the aureole data and 0.35, (0.05), 1.05 μm for the extinction data. No observational errors are involved. Even for such ideal conditions, the value of the refractive index cannot be obtained accurately from the aureole and extinction measurements if the absolute values of the aureole data are not available. We therefore assume an *a priori* value of $m = 1.50 - 0.01i$ for the refractive index of aerosols in the following analyses.

The aureole intensity and the optical thickness have been measured in the program of solar radiation and aerosol measurements informally organized by groups from Tohoku University and the Meteorological Research Institute during the periods of 4–7 Nov. 1978 and 1–3 Nov. 1979 in Sendai, Japan. The aureole meter consists of a telescope mounted on an equatorial driven by a clock motor. The equatorial is further mounted on a horizontal turntable. By this configuration the aureole meter can scan a circle of equizenith angle of the sun during observation. The object lens with 65-mm diam is shaded from the direct solar radiation by a 75-cm long hood. The shapes of the window of the sun-shading hood and the field stop are rectangular as proposed by Twitty *et al.*[17] The light signals are detected by a photodiode (S-640, Hamamatsu TV Corp.) after passing the interference filters with peak transmission wavelengths of 0.560, 0.788, and 1.040 μm.

Figure 8 shows the aerosol phase functions retrieved from observed data in 1979 normalized at the scattering angle of 5°. Figure 9 shows the optical thickness of aerosols simultaneously obtained from the extinction measurements of the direct solar radiation by a sun photometer. The sun photometer used is a modified version of Model MS-7 (EKO Instruments Trading Co., Ltd.) with wavelengths of 0.369, 0.500, 0.675, 0.776, and 0.862 μm. We can see from these figures that the concentration and the size distribution of aerosols were relatively stable on each day, although some daily variation was observed. We can also see that the normalized phase functions were relatively independent of wavelength and the optical thicknesses were approximately proportional to the reciprocal of wavelength, suggesting that the size distributions of aerosols nearly obeyed the Junge power law with $p = 4$. The volume spectra of aerosols retrieved by the simultaneous inversion of these data are shown in Fig. 10. The reliability of inverted size distribution is restricted

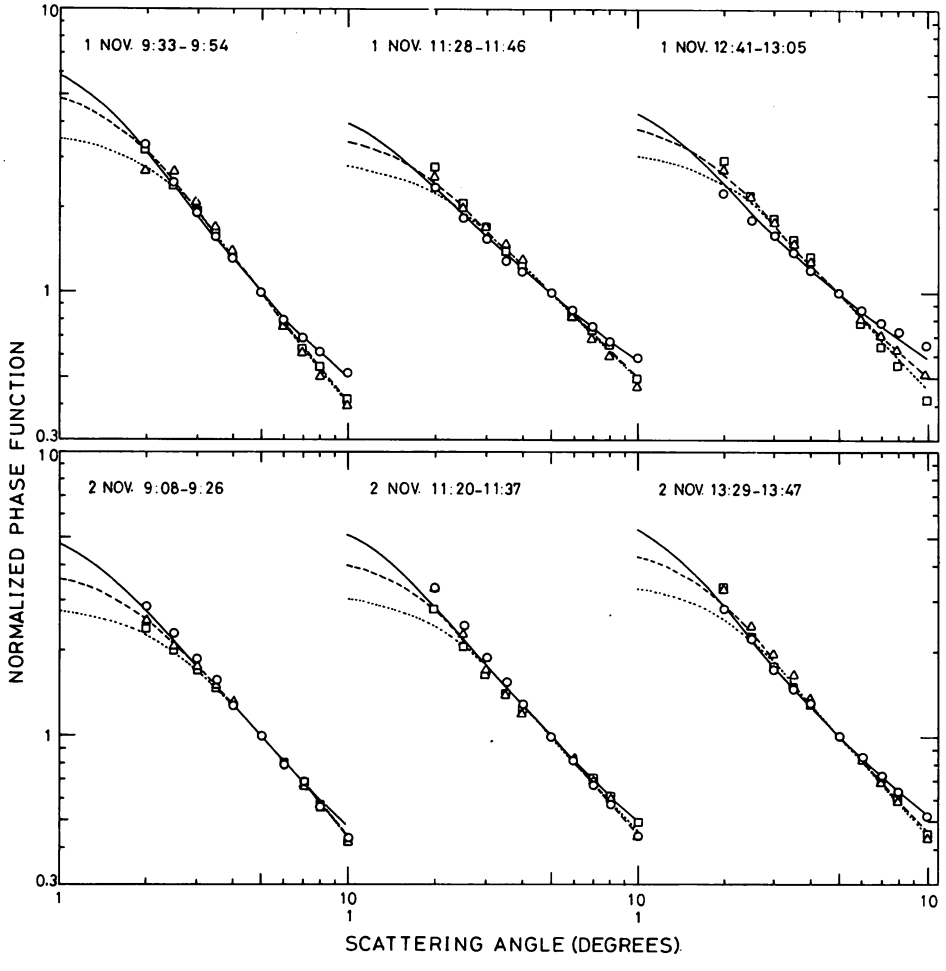

Fig. 8. Forward parts of the phase functions of aerosols obtained from observations of 1,2 Nov. 1979. Data are normalized at $\Theta = 5°$. Symbols and lines are retrieved and reconstructed phase functions, respectively. Wavelengths are 0.560 (—○—), 0.788 (---△---), and 1.040 μm (·····□·····), respectively.

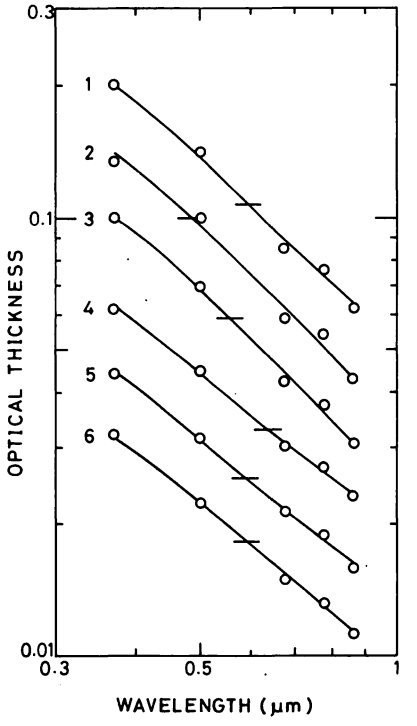

Fig. 9. Observed (O) and reconstructed (—) spectral optical thicknesses of aerosols corresponding to the six phase functions shown in Fig. 8. The horizontal bar attached to each profile shows the value of 0.1 (or 0.2) for the data on 1 Nov. (or 2 Nov.).

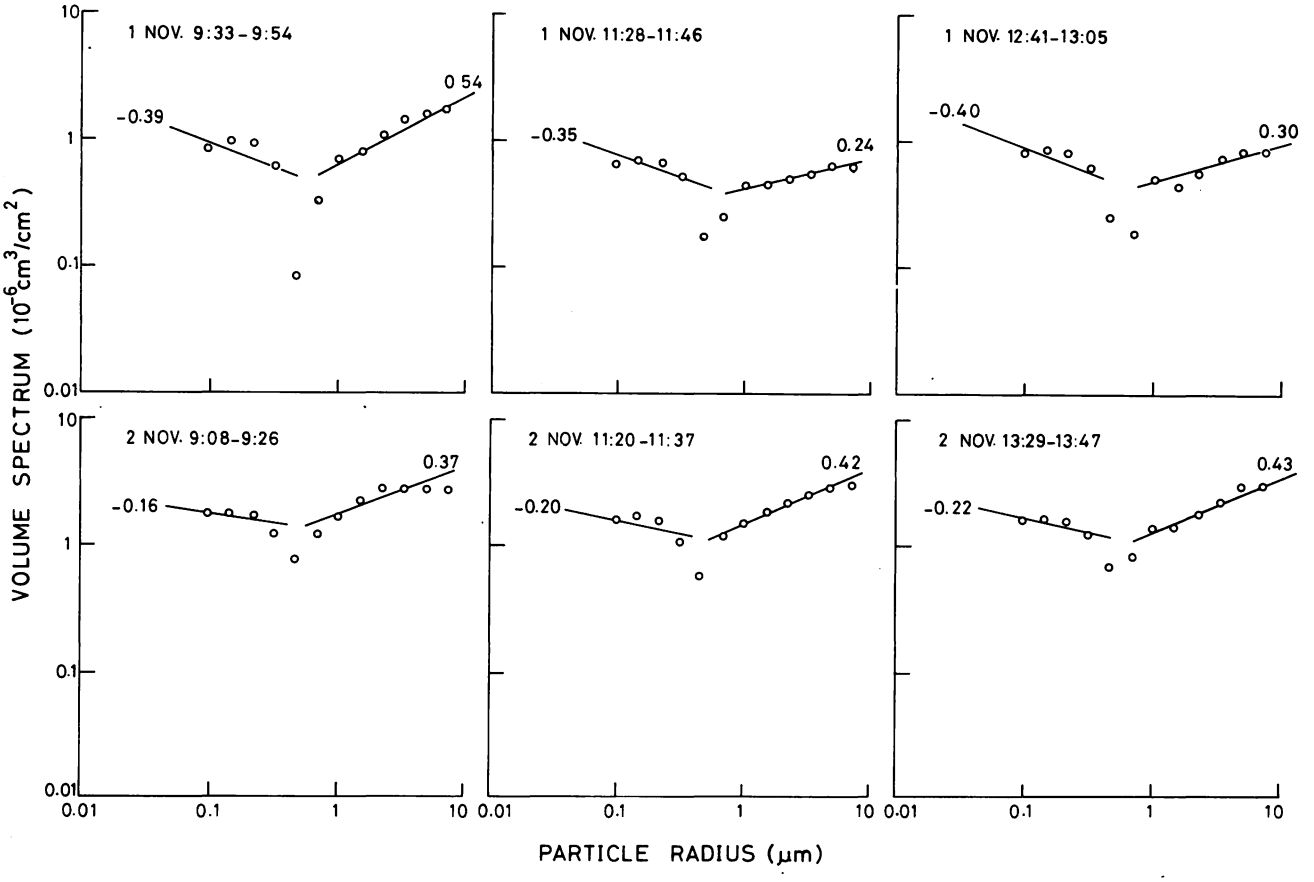

Fig. 10. Volume spectra of aerosols retrieved by the simultaneous inversion of the data shown in Figs. 8 and 9 (circles). Approximate estimations of the exponent of the power-law approximation by Eq. (27) are also shown by solid lines with values of $4 - p$.

within the size range where the maximum contribution of a spectral portion to any portions of observed optical quantities exceeds the limit of 10%, i.e., $C_{max} \gtrsim 0.1$.[15] Figure 10 shows that meaningful volume spectra can be retrieved in the size range of radii from ~0.1 to 10 μm, where C_{max} is larger than 0.1. All spectra shown in Fig. 10 exhibit a bimodal feature with smaller and larger size branches. The branch of smaller particles has its maximum around $a = 0.13$ μm and $1/e$ width of 1.8 when we approximate the branch by a lognormal distribution, which corresponds to the Mode C aerosols of Patterson and Gillette.[18] Since the branch of larger particles extends beyond the size range of analysis, the mode radius and $1/e$ width cannot be determined. As mentioned before, if we approximate the size distribution of aerosols by the power law of the form $v(\ln a) = C \times a^{4-p}$, we can obtain the exponent $4 - p$ from wavelength dependence of the aerosol optical thickness and scattering angle dependence of the aerosol phase function by use of Eq. (27). The solid lines in Fig. 10 show the volume spectra thus obtained. The solid lines for the smaller particles show the volume spectra obtained from the optical thickness data, and those for the larger particles from the phase function data. Since the absolute values of the volume spectra cannot be determined from our normalized data, relative values are plotted to fit the inversion results. In general, the values of the exponent p obtained from the optical thickness data and the phase function data do not coincide with each other and represent respective portions of the size spectrum, being consistent with inversion results. Thus, very useful information of the aerosol volume spectrum can be extracted from simultaneous measurements of the direct and circumsolar radiation.

V. Summary

We have developed a method of calculating the intensity of scattered radiation in the solar aureole region as well as a method of inverting the aerosol volume spectrum from direct and circumsolar radiation measurements. Results obtained are (1) distribution of the circumsolar radiation can be calculated with accuracy of about ±3% for $\tau_a \lesssim 1$ and $\xi \lesssim 5$ if we adopt $M = 7$ in Eq. (12); (2) relative values of the aerosol phase function can be retrieved fairly accurately even for atmospheric conditions with significant multiple scattering, whereas absolute values of the phase function cannot be retrieved unless we know the single scattering albedo of aerosols as well as their optical thickness; and (3) the aerosol volume spectrum retrieved from the observation showed a bimodal feature which can also be inferred approximately from the simple parameter fitting in Eq. (27).

Simultaneous measurements of the direct and circumsolar radiation are very promising for the remote sensing of the optical properties of aerosols since information on the extinction and scattering abilities of aerosols is contained independently in the data and both data are columnar quantities along the same slant path. It is an important future problem to develop a technique to retrieve the absolute value of the aerosol phase function from which we can estimate the absorption cross section of aerosols. Data of known spectral intensities of Rayleigh scattering[17] or the twenty-two halo of cirrus clouds will be valuable for the calibration of the instrument.

References

1. J. A. Weinman, J. T. Twitty, S. R. Browning, and B. M. Herman, J. Atmos. Sci. **32**, 577 (1975).
2. M. A. Box and A. Deepak, J. Atmos. Sci. **38**, 1037 (1981).
3. J. E. Hansen, J. Atmos. Sci. **26**, 478 (1969).
4. J. F. Potter, J. Atmos. Sci. **37**, 868 (1970).
5. G. E. Shaw, Appl. Opt. **18**, 988 (1979).
6. T. Nakajima, "Solar Radiative Transfer in the Atmosphere–Ocean System," Science Dr. Thesis, Department of Science, Tohoku U., Sendai (1980).
7. A. Deepak, G. P. Box, and M. A. Box, Appl. Opt. **21**, 2236 (1982).
8. K. Arao, "Rigorous Solutions of Solar Aureole in Turbid Atmospheres," Science Dr. Thesis, Department of Science, Tohoku U., Sendai (1978).
9. D. Deirmendjian, 1970 [cited in M. A. Box and A. Deepak, J. Atmos. Sci. **38**, 1037 (1981)].
10. J. H. Joseph, W. J. Wiscombe, and J. A. Weinman, J. Atmos. Sci. **33**, 2452 (1976).
11. W. J. Wiscombe, J. Atmos. Sci. **34**, 1408 (1977).
12. M. Tanaka and T. Nakajima, J. Quant. Spectrosc. Radiat. Transfer **18**, 92 (1977).
13. W. J. Wiscombe and J. W. Evans, J. Comput. Phys. **24**, 416 (1977).
14. T. Nakajima and S. Asano, Sci. Rep. Tohoku Univ. **24**, 89 (1977).
15. M. Tanaka, T. Nakajima, and T. Takamura, J. Meteorol. Soc. Jpn. **60**, 1259 (1982).
16. S. Twomey, J. Assoc. Comput. Mach. **10**, 97 (1963).
17. J. T. Twitty, R. J. Parent, J. A. Weinman, and E. W. Eloranta, Appl. Opt. **15**, 980 (1976).
18. E. M. Patterson and D. A. Gillette, J. Geophys. Res. **82**, 2074 (1977).

This study was supported by Research Project, grant-in-aid for Scientific Research of the Ministry of Education, Science, and Culture, Japan, project 474179. The authors wish to thank K. Arao for providing the exact values of intensity distribution in the solar aureole calculated by the matrix method. The authors also thank the staff of the Sendai Astronomical Observatory for use of facilities and Y. Nakanishi of EKO Instruments Trading Co., Ltd. for technical assistance.